Received: 18 September 2018 | Revised: 25 January 2019 | Accepted: 5 February 2019

DOI: 10.1002/stc.2346

RESEARCH ARTICLE

WILEY

Performance-based seismic design of tuned inerter dampers

Alin Radu | Irina F. Lazar | Simon A. Neild

School of Civil, Aerospace and Mechanical Engineering, University of Bristol, Bristol, UK

Correspondence
Alin Radu, School of Civil, Aerospace and Mechanical Engineering, University Walk, Bristol BS8 1TR, UK.
Email: alin.radu@bristol.ac.uk

Funding information
Engineering and Physical Sciences Research Council, Grant/Award Number: EP/K005375/1; H2020 Marie Skłodowska-Curie Actions, Grant/Award Number: 704679 - PARTNER

Summary

This paper proposes a novel fully probabilistic framework for the performance-based seismic design of structures and uses tuned inerter dampers (TID) installed in civil engineering structures subjected to seismic loads to illustrate its applicability. The framework proposed is based on stochastic reduced-order models, which makes it computationally efficient and can be used for the design of TIDs installed in any complex nonlinear structures subjected to general nonstationary, non-Gaussian stochastic processes. In this study, the TID is installed in a multi-degree-of-freedom nonlinear structure that is subjected to synthetic seismic records. Numerical results show that the framework proposed is able to provide rigorous and robust values for the parameters of the TID. The design parameters obtained using the stochastic framework proposed are compared with benchmark deterministic approaches, tested also for a large data set of ground-motion real records. It is shown that the stochastic approach provides insightful designs of the TID that are consistent with the site seismicity and the frequency content of the stochastic excitation.

KEYWORDS

control engineering, earthquake-risk reduction, performance-based engineering, stochastic reduced-order models, tuned inerter damper, vibration suppression

1 | INTRODUCTION

Vibration-suppression systems have been used for decades to protect structures against potential damage caused by seismic loads. In addition to already-classical devices, such as viscous dampers (VD)[1-3] or tuned mass dampers,[4-6] novel devices, such as tuned mass-damper inerters (TMDI)[7] or tuned inerter dampers (TID)[8] have been proposed to address this problem in recent years. These devices incorporate inerters,[9] devices that are able to generate forces proportional to the relative accelerations between their nodes. TMDIs, similar to TMDs, are mass-spring-damper single-degree-of-freedom (SDOF) systems, but with an additional inerter, meant to supplement and/or substitute part of the TMD's mass and connected across two structure attachment points, like a damper. Compared with the TMDI, the TID have a simpler configuration that, besides the mass of the device itself, substitutes the entire active mass of the TMD for an inerter, which is mounted in series with a spring and a damper. All these three systems, the TMD, the TID, and the TMDI, could be installed in multi-degree-of-freedom (MDOF) systems, and due to their setup, they would introduce an additional DOF in the original system. Other configurations involving inerters, such as Ikago et al.[10] who introduced a tuned viscous mass damper for civil engineering applications,[11] have been proposed in the literature and are discussed by Zhang et al.[12]

In addition to the earlier studies demonstrating how TIDs can be designed to improve the behaviour of host structures, such as multistorey buildings[8] or stay cables,[13] TIDs have also been tested experimentally using dynamic substructuring[14] emphasising their feasibility and applicability. Besides civil engineering design applications,[12,15,16] inerter-based vibration absorbers have been considered in the context of a range of practical applications, such as vehicle suspensions,[17-19] train suspensions,[20,21] or aircraft landing gears.[22] The majority of the studies on optimal control devices of the kind presented herein consider frequency or time-domain analyses that involve the calculation of multiple structural system's response.

The aim of this study is to propose a novel, general, accurate, yet efficient, fully probabilistic framework for the performance-based design of vibration control systems, such as the ones enumerated above, for civil engineering structures subjected to seismic loads. Once presented, the proposed methodology is then demonstrated using the example of the probabilistic seismic design of a TID. Even though the framework is discussed through the use of this example, it allows for the structural system, the vibration control device, and the input to be replaced by customised models relevant to other applications. Nevertheless, the example shown uses a rather general case of a TID installed in a nonlinear MDOF structure subjected to a non-Gaussian, nonstationary stochastic process.

The seismic performance design of structures is a challenging problem for the following reasons: The number of available earthquake records is insufficient even in high-seismicity areas,[23] and performing dynamic analyses for realistic complex structures is strenuous. These issues have been discussed extensively in the literature, and approximate methods were proposed to overcome them. It is common to use real ground-motion records from large data sets selected to be consistent with specified spectral values of the response.[24-26] The limitations regarding the small number of records available are often resolved by methods involving scaling recorded earthquake time histories to common intensity measures. One popular approach, known as the incremental dynamic analysis (IDA) and presented by Vamvatsikos et al.,[27] involves repeated scaling of seismic ground motions to increasing intensity measures until the specified damage state is reached. This method may yield unsatisfactory results for some nonlinear systems.[28,29] The limitations of scaling ground motions[30] may be resolved by simulating synthetic ground motions, an approach that has already been adopted in the performance-based seismic analysis of structures.[29,31]

The issue of calculating the response of dynamic systems in the general nonlinear systems subjected to nonstationary, non-Gaussian input, because the framework of the random-vibration theory can not be used in complex realistic applications. The general random-vibration theory is insufficient to perform this task,[32] because it can only provide solutions for second-moment properties of the states of arbitrary linear systems subjected to Gaussian random input. Most applications of inerter-based systems were studied in a deterministic framework, where closed form solutions can be found for simplified structures and excitation patterns,[8,33-35] or numerically,[13,14] for more complex scenarios. Some studies used elements of random-vibration theory to design inerter-based vibration-control systems,[36-38] but by adopting this approach, they were limited to linear structures subjected to Gaussian stationary excitations. In a similar context, Masri et al.[39,40] develop relations for the covariance of the response of linear SDOF or MDOF subjected to amplitude-modulated nonstationary Gaussian white noise. Other studies, among which, Wang and Su[41] study nonlinearities of inerters in a similar context by using approximate linear transfer functions. These are just a few examples of analytical relations developed for simplified scenarios of linear or linearised systems subjected to Gaussian white or non-white noise. An early comparison of benchmark methods for the characterisation of the dynamic response of nonlinear MDOF structures is presented by Bazzurro et al.[42] More solutions for dealing with the computational complexity of resolving structural systems were proposed by assuming that the structures behaved linearly,[43,44] by linearization of nonlinear structural systems,[45-47] or by using a reduced number of modes of vibration in the response analyses.[48,49] Monte Carlo (MC) is the only general numerical method available for solving complex nonlinear dynamic systems subjected to complex stochastic input and is widely used in many applications. However, the MC solution is computationally expensive, arguably prohibitive so, when applied to the design of complex realistic nonlinear systems[50,51] because it requires repeated deterministic dynamic analyses for many random ground-motion samples. The development of efficient alternatives to MC method has been a topic that has drawn a lot of attention over the years, with various applications, among which a few examples are the quasi MC simulation,[50,52] Latin hypercube,[53] the change of measure[54] (Section 5.4), the equivalent stochastic linearisations,[55] the stochastic averaging method,[56] or reduced orders of the nonlinear system by using linear or nonlinear normal modes.[57,58]

The framework proposed in this paper for the seismic performance-based design of the TID relies on stochastic reduced order models (SROMs).[59] SROMs are stochastic processes defined by a relatively small number of unequally-likely samples that fully characterize the probability law of that process. The samples of the SROM are selected such that they reduce the differences between the SROM and the original input process. Thus, only the small number of optimally selected SROM samples are used for the dynamic analyses —this significantly reduces the number of analyses required by the MC method. The method was originally developed for dynamic response,[60] and recently, it was shown that it can be extended[61] and

through further refinements can now be used to solve stochastic differential equations.[62] Here, the proposed framework uses an SROM for the seismic input, enabling response statistics to be used as design criteria. The metric used for the design of the TID is defined with respect to the tail distribution of the engineering demand parameters. The sensitivity between the MC and the SROM response statistics is also analysed in order to establish the accuracy and robustness of the method proposed.

The current paper is structured in three main parts. In the first part, the performance-based seismic design framework is described with respect to the structural system chosen: a TID installed in a MDOF nonlinear system. The performance criterion for the design of the TID is to reduce the area under the tail distribution of the maximum displacement of the structural system beyond a critical displacement value, or in other words, to minimise the probability of exceeding a critical maximum displacement. The second part of the paper consists of a description of the seismic hazard to which the structure is subjected. Synthetic ground-motion records are used for the dynamic analyses. These records are samples of nonstationary, non-Gaussian stochastic processes, defined as a function of moment magnitudes, and source-to-site distances. The construction of the SROM for the earthquake excitation model is also described in this section. Finally, in the last part of the paper, numerical results that examine the performance of the TID as the structure is exposed to the SROM excitation samples are shown, and a methodology of selecting the design parameters of the TID is shown in detail. The paper concludes with a discussion of the methodology proposed with respect to benchmark studies and current practices.

2 | PERFORMANCE-BASED SEISMIC DESIGN

The current paper proposes a general framework for the performance-based seismic design of TIDs, installed in structures subjected to earthquake loads. It is important to note that the vibration-suppression performance-based design problem addressed herein is general and can be applied to any type of stable nonlinear structures and stochastic loads, characterised by their probability law or samples. Here, the design of the TID is performed for a general scenario of a nonlinear MDOF system subjected to nonstationary, non-Gaussian seismic input to demonstrate the proposed approach.

In the context of the performance-based framework, the design parameters of the TID, as defined later in this section, will be selected based on the overall performance of the structural system, in terms of the system's response statistics. Let us denote the response of the structural system altered by a TID with parameters θ_D and subjected to the stochastic process $A(t)$, by $X(t;\theta_D)$. Then, the design parameters of the TID, θ_D, will be selected by minimising a cost function $\varphi(\theta_D)$. Function $\varphi(\theta_D)$ can describe any statistics of the response, for example, the statistical moments or quantiles of engineering demand parameters (e.g., the maximum displacement or the interstorey drift) as functions of the response $X(t;\theta_D)$. For convenience, the notation of the dependence of the controlled system's response on θ_D will not be carried on.

2.1 | Structural system

We assume that the TID is installed in a nonlinear MDOF structure. Specifically, the example structure we consider is a N_{dof}-DOF system with a cubic nonlinearity, whose response is represented by the vector $X(t) = \{X_i(t), i = 1, \dots, N_{dof}\}$ of dimension $(N_{dof}, 1)$, described by the following equation of motion:

$$M\ddot{X}(t) + C\dot{X}(t) + K\left(X(t) + \rho X_{(3)}(t)\right) = -M\underline{1}A(t), \tag{1}$$

where $M = \{m_{i,j}|m_{i,i} > 0; m_{i,j} = 0, i \neq j; i,j = 1, \dots, N_{dof}\}$, $C = \{c_{i,j}|c_{i,j} = c_{j,i}; i,j = 1, \dots, N_{dof}\}$, and $K = \{k_{i,j}|k_{i,j} = k_{j,i}; i,j = 1, \dots, N_{dof}\}$ are the mass, damping, and stiffness matrices; vector $\underline{1}$ is a unit vector of dimension $(N_{dof}, 1)$; parameter ρ is a nonlinear parameter; and $A(t)$ is a stochastic process that describes the seismic input to which the structure is subjected. The input $A(t)$ will be described in detail in the next section. Note that the vector $X(t)_{(3)} = \{X_i(t)^3, i = 1, \dots, N_{dof}\}$ denotes an element-wise power of the vector $X(t)$. For the numerical example in this paper, the MDOF used has $N_{dof} = 5$ DOF, and specific values for the structural system assumed are presented in the Appendix. Figure 1 shows the backbone curves of the first and the fifth DOF, that is, $\max_{t\geq 0}|X_1(t)|$ and $\max_{t\geq 0}|X_5(t)|$, for which $X(t)$ is the response of the structural system subjected to $A(t) = a_0 \sin(\nu t)$. Note that the backbone curves are plotted against the ratio between the harmonic frequency ν and the dominant frequency of vibration of the structural system. As seen in Figure 1, the system exhibits a softening behaviour as the amplitude a_0 of the harmonic loading increases, which is typical for buildings.[63]

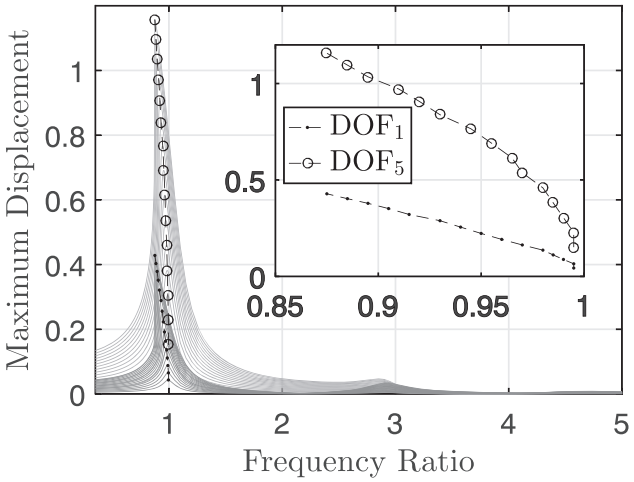

FIGURE 1 Backbone curves for the first (DOF_1) and the fifth (DOF_5) DOF_s

2.2 | Tuned inetrer damper

The aim of this paper is to propose a novel, computationally efficient framework to perform a seismic performance-based design of passive vibration-control systems, and we demonstrate how to use this framework for the design of a TID installed in an MDOF nonlinear structure subjected to seismic loads, as defined in Equation 1. The TID, as already described in Section 1, is a passive vibration-suppression device, explored previously in civil engineering theoretical and experimental studies for the same purpose as other passive vibration-control systems, such as the VD, or the tunedmass dampers (TMD), to reduce vibrations in structures. The TID combines the advantages of both the VD and the TMD.[8] Like the TMD, the TID introduced an additional DOF to the structure, with additional damping and stiffness. Unlike the TMD, the TID's physical mass is replaced by an apparent mass produced by the inerter, and similar to the VD, the TID is connected to two terminals of the structure. Thus, the TID is able to reduce the system's response at the main frequency, similar to the TMD, and the response at the other secondary frequencies, similar to the VD. The TID as defined by Lazar et al.,[8] is described by three parameters $\theta_D = [m_D, \nu_D, \zeta_D]$. The additional DOF introduced by the TID into the structural system is characterised by the apparent mass m_D, the frequency ν_D, and the damping ratio ζ_D.

The equation of motion of the structural system equipped with a TID described by the parameters θ_D is similar to Equation 1 with the response vector $X(t) = \{X_i(t), i = 1, \dots, N_{dof} + 1\}$, for which $X_{N_{dof}+1}$ corresponds to the additional DOF introduced by the TID. The mass matrix M is replaced by $M^{(d)} = \{m^{(d)}_{i,j}, \quad i, j = 1, \dots, N_{dof} + 1\}$, constructed by adding the apparent mass of m_D of the additional DOF corresponding to the TID. Similarly, the damping and the stiffness matrices C and K are replaced by $C^{(d)} = \{c^{(d)}_{i,j}, \quad i, j = 1, \dots, N_{dof} + 1\}$ and $K^{(d)} = \{k^{(d)}_{i,j}, \quad i, j = 1, \dots, N_{dof} + 1\}$, respectively, by using the damping $c_D = 2m_D\zeta_D\nu_D$ and stiffness $k^{(d)} = m_D\nu_D^2$ of the TID. For a clearer understanding of how the TID affects the structural behaviour of the MDOF structure, the modified mass $M^{(d)}$, damping $C^{(d)}$, and stiffness $K^{(d)}$ matrices are shown in matrix form as a function of the original matrices M, C, and K, respectively, in the Appendix. Note that implicitly the vector $\underline{1}$ in this new equation of motion Equation 1 also has the dimension $(N_{dof} + 1, 1)$.

The design of the TID consists of finding parameters θ_D with respect to a performance criteria as a function of the structural system's response $X(t)$. The apparent mass $m_D = \mu_D \sum_{i=1}^{N_{dof}} m_{i,i}$ is a characteristic of the inerter, which is commonly chosen by the designer when selecting the type of inerter used. A value of $\mu_D = 20\%$ is selected a priori to account for the capability of the inerter to generate an increased apparent mass. By comparison with the traditional TMD's mass that can go up to a maximum of 10% of the host structure's mass, the value $\mu_D = 20\%$ being only two times larger is reasonable compared with larger values reported in the literature.[9] Thus, the design of the TID reduces to the calculation of just two parameters (ν_D, ζ_D), based on the performance criterion defined by the minimisation of a cost function $\varphi(\nu_D, \zeta_D)$. For the purpose of this paper, we define the cost function as

$$\varphi(\nu_D, \zeta_D) = \int_{x_{cr}}^{\infty} (1 - F_X(x))\, dx, \tag{2}$$

where $F_X(x) = \mathbf{P}\{\max_{t\geq 0}|X_5(t)| \leq x\}$ is the probability distribution function of the maximum displacement of the controlled structure $X(t)$, for a given set of parameters (ν_D, ζ_D). Note that the maximum absolute displacement $\max_{t\geq 0}|X_5(t)|$ can be replaced by any other engineering demand parameter, such as the maximum absolute interstorey drift $\max_{t\geq 0}|X_i(t) - X_{i+1}(t)|, \quad i = 1, \ldots, N_{dof} - 1$. The optimum design parameters (ν_D, ζ_D) will be given by the minimum value of $\varphi(\nu_D, \zeta_D)$, over a range of values for (ν_D, ζ_D). This range is chosen such that the damping and stiffness parameters remain realistic from a practical point of view. A maximum damping ratio $\zeta_D = 30\%$ and a maximum frequency $\nu_D = 8\pi\, rad/s$ are assumed.

3 | SEISMIC HAZARD

Large numbers of ground-motion records are required to perform probabilistic analyses for the response of structures to earthquakes. The seismic-hazard model used for the seismic performance-based design proposed in this study has two main components: (a) the distribution of earthquakes with respect to the moment magnitude m and the source-to-site distance r; and (b) the ground-motion model for the simulation of ground-motion time histories, as a function of (m, r), and other secondary parameters. The (m, r) distribution of the seismic hazard is essential in the seismic design of structures because the frequency content of the ground motions depends on (m, r), among other characteristics, such as local site conditions or seismic regime.[29,64]

The distribution of earthquakes by (m, r) is obtained from the UHT[65] from the United States Geological Survey. This online tool provides the contribution of the seismic sources characterized by (m, r) for a specified level of the seismic intensity (e.g., the spectral acceleration) at each site in the United States. This $(m, r)-$distribution is also known as the seismic disaggregation defined in detail by McGuirre[66] and Bazzurro and Cornell.[67] For the numerical example in this study, downtown Los Angeles with a shear velocity in the top $30m$ of soil of $v_{s30} = 760\, m/s$ is chosen as the site for the design of the TID. Note that in our methodology, we utilise the UHT's disaggregation only to extract the contribution of

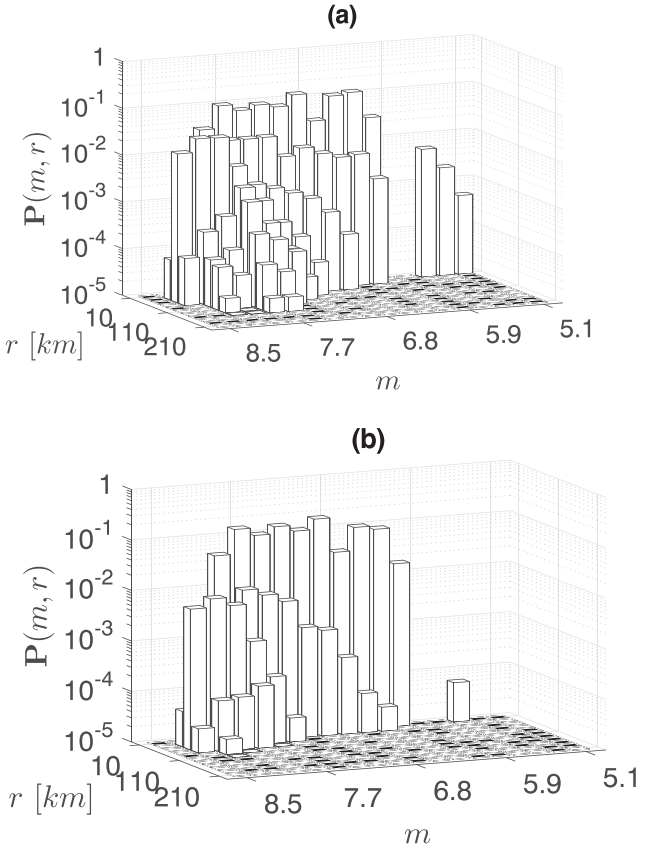

FIGURE 2 Seismic activity matrices for Los Angeles, for the probability of exceedance of (a) 10% and (b) 2% in 50 years, with $v_{s30} = 760 m/s$

each source characterised by (m, r) at a given site. For convenience, we selected just (m, r)-earthquakes that correspond to a probability of occurrence equal to or larger than 10^{-5}, which is achieved for $m \geq 5$ and $r \leq 100\,km$. The normalised values of contributions of each pair (m, r) result in the probability mass function for the bivariate vector (M, R), where M and R are the random variables corresponding to the moment magnitude m and source-to-site distance r, also known as the seismic activity matrix.[23] We denote by $\mathbf{P}\{(M, R) = (m, r)\}$ the probability of occurrence of an earthquake characterised by (m, r). Figure 2 shows the seismic activity matrices for downtown Los Angeles, obtained from the UHT's disaggregation for a level of the hazard characterized by a probability of exceedance of (a) 10% and (b) 2% in 50 years, respectively.

3.1 | Ground-motion simulation

The ground-motion model used in this study allows the simulation of synthetic earthquakes as a functions of (m, r), local soil conditions in term of v_{s30} and seismic regime. The model is based on the specific barrier model (SBM)[68,69] and the spectral representation methods.[54,70] The synthetic motions are samples of a nonstationary, non-Gaussian stochastic process $A(t)$ with finite duration t_f:

$$A(t) = h(t)Z(t), \quad 0 \leq t \leq t_f, \tag{3}$$

where

$$h(t) = \alpha t^{\beta} \exp\{-\gamma t\} \tag{4}$$

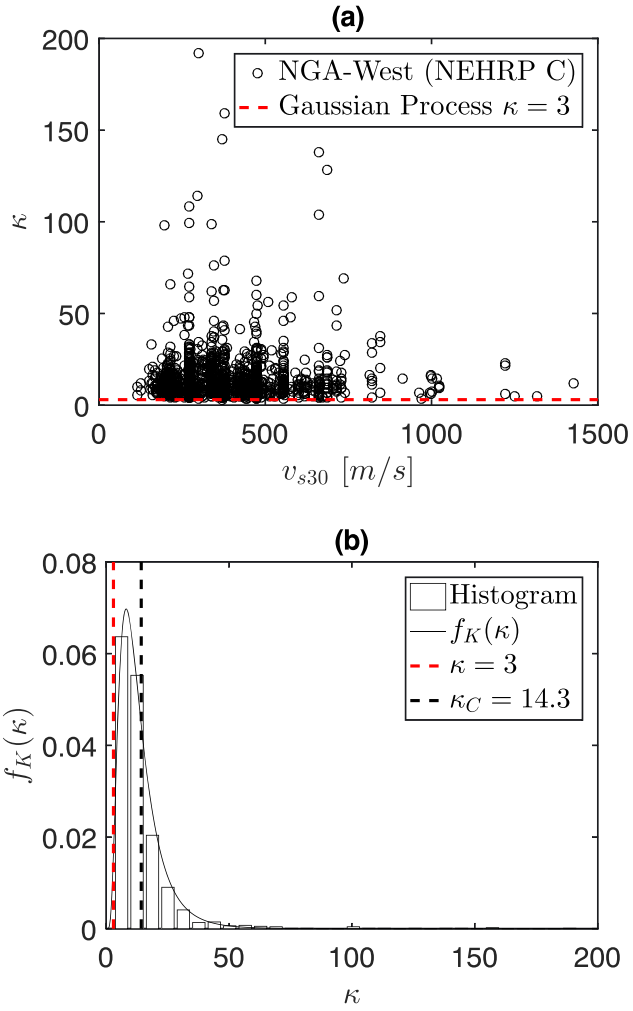

FIGURE 3 (a) Scatter plot of the kurtosis coefficient κ versus v_{s30} and (b) probability density function of κ for type-C NEHRP soil

is a deterministic amplitude-modulation function with constant parameters α, β, and γ. The process $Z(t)$ is a zero-mean, stationary, process with a Student's T marginal distribution. The second-order moment properties of $Z(t)$ are given by the one-sided spectral density function $g(\nu; m, r)$, $\nu \geq 0$ obtained from the SBM calibrated to global data[71] or calibrated to site records by Radu and Grigoriu.[23] Parameters α, β, γ in Equation 4 and the duration $0 \leq t \leq t_f$ are also functions of (m, r), and are outputs of the SBM. The model in Equation 3 is a simplified version of the ground-motion model introduced by Radu and Grigoriu.[64]

The advantage of using the model in Equation 3 is due to the fact that it preserves the realistic non-Gaussian character of earthquakes, a feature usually not considered in other models.[31,72] The non-Gaussianity of real earthquakes is supported by the results in Figure 3a, which show that the kurtosis coefficient as a function of v_{s30} for the ground motions in the NGA-West data set[73] is greater than 3, the characteristic value for Gaussian processes. Figure 3b shows the probability distribution function of the kurtosis κ for the type-C National Earthquake Hazard Reduction Program (NEHRP) soil, similar to the soil assumed for this study. The distribution of $Z(t)$ is calibrated to the average kurtosis coefficient corresponding to type-C NEHRP soil $\kappa_C = 14.3 >> 3$ as shown by Radu and Grigoriu.[64]

Figure 4a illustrates the power-spectral density functions $g(\nu; m, r)$ for three pairs of $(m, r) = (6.3, 30\,km)$, $(m, r) = (7.5, 70\,km)$, and $(m, r) = (8.1, 110\,km)$, for $v_{s30} = 760\,m/s$, which shows that the frequency content of the motion is dependent on (m, r). Figure 4b shows time-history samples of $A(t)$ in Equation 3 for the three pairs of (m, r) in (a), with their corresponding frequency contents and lengths t_f.

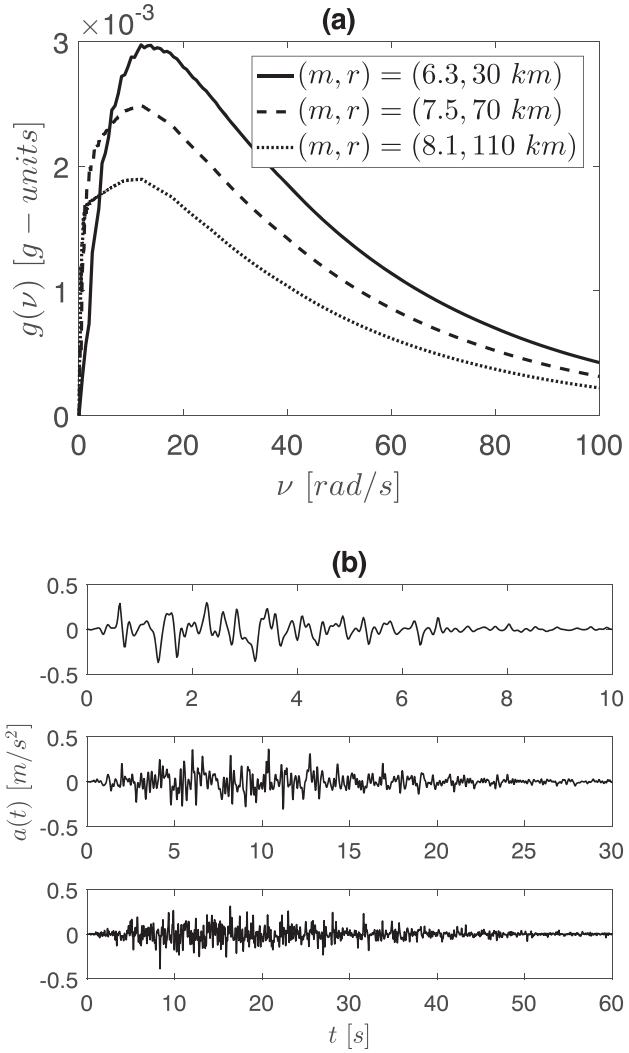

FIGURE 4 (a) Power spectral density functions $g(\nu; m, r)$, (b) samples of $A(t$; from top to bottom) for $(m, r) = (6.3, 30\,km)$, $(m, r) = (7.5, 70\,km)$, and $(m, r) = (8.1, 110\,km)$, respectively

Other ground-motion stochastic simulation models such as the ones proposed by Rezaeian and Kiureghian[31,72] or Vlachos et al.,[74] or more complex physics-based models such as Goda et al.,[75] can be used to simulate earthquakes as functions of (m, r), and so can be substitutes of the model adopted in this study, within our proposed framework. Irrespective of whether the substitute model is fully defined or just its samples are available, it suffice to just build the respective SROM based on sample statistics.

3.2 | SROM for seismic input

As discussed before, a large number of samples of $X(t)$, for each pair of the TID parameters $(\nu_D; \zeta_D)$, are necessary to obtain reliable values for the design metric in Equation 2. This would imply a significant computational effort, because each sample of $X(t)$ is obtained through the solution of Equation 1 for a sample of $A(t)$. Thus, in order to resolve this issue, an SROM for the earthquake process $A(t)$ is constructed. An SROM $\tilde{A}(t)$ of $A(t)$ is defined by any number $\tilde{n}$ of samples $\tilde{a}_k(t)$ of $A(t)$ with probabilities p_k such that $\sum_{k=1}^{\tilde{n}} p_k = 1$. Similar to MC, the SROM also uses random samples of $A(t)$, but unlike in the case of MC, the samples are not equally likely but weighed by distinct probabilities. Pairs of $A(t)$ samples and their probabilities, $\{(\tilde{a}_k(t), p_k), \quad k = 1, \ldots, \tilde{n}\}$, are selected such that $A(t)$ and $\tilde{A}(t)$ have similar probability laws. It was shown by Grigoriu[60,76] that it is possible to select a relatively small number $\tilde{n}$ of independent samples of $A(t)$ to construct an SROM $\tilde{A}(t)$. Our objective is to find p_k such that the discrepancies between the probability laws of the SROM $\tilde{A}(t) = \{(\tilde{a}_k(t), p_k), \quad k = 1, \ldots, \tilde{n}\}$ and $A(t)$ are minimized. The probability laws of stochastic processes are defined by their moments, marginal distributions, and covariance functions.[77] The target marginal distribution $F(x; t)$, moments $\mu(t; q)$ of order q, and covariance function $\Sigma(t, s)$ of $A(t)$ can be calculated directly from its samples or directly from the definition in Equation 3. The same statistics for the SROM $\tilde{A}(t)$ are calculated from its $\tilde{n}$ samples $\tilde{a}_k(t)$, weighed by their probabilities p_k. Thus, the moments $\tilde{\mu}(t; q)$ of order q, the marginal distribution $\tilde{F}(x; t)$, and the covariance function $\tilde{\Sigma}(t, s)$ of the SROM $\tilde{A}(t)$ are calculated respectively as follows:

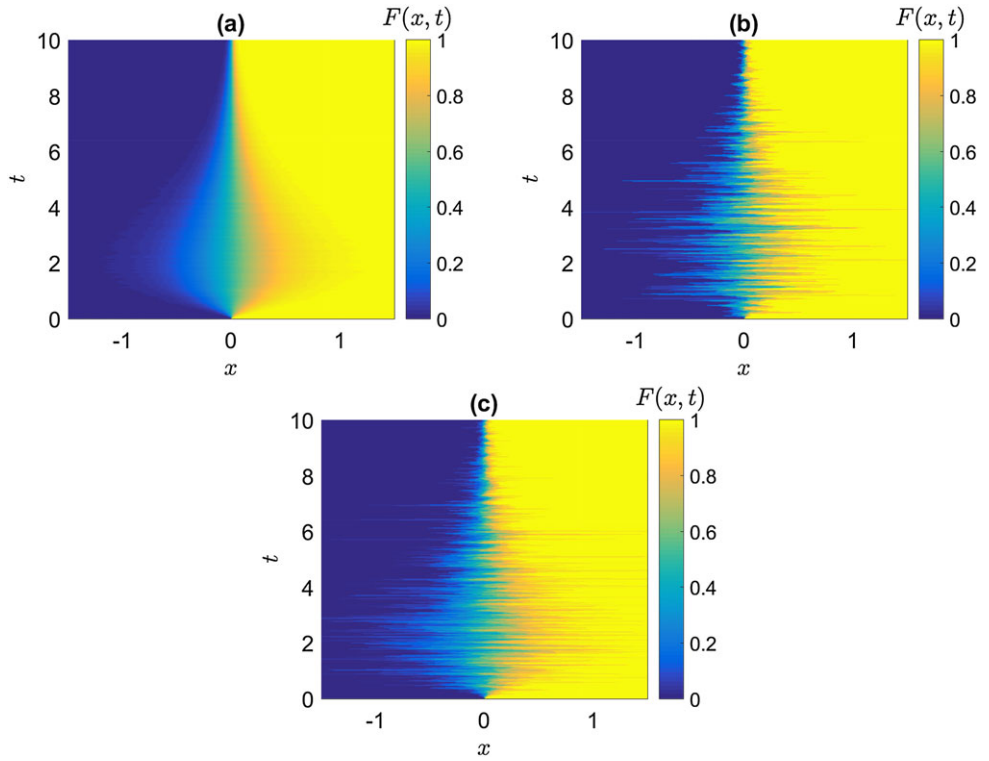

FIGURE 5 Marginal distributions (a) $F(x, t)$ for $n = 5,000$ samples of $A(t)$; and the SROM estimates $\tilde{F}(x, t)$ for (b) $\tilde{n} = 10$ and (c) $\tilde{n} = 20$, for $A(t)$ calculated using $(m, r) = (6.3, 30km)$

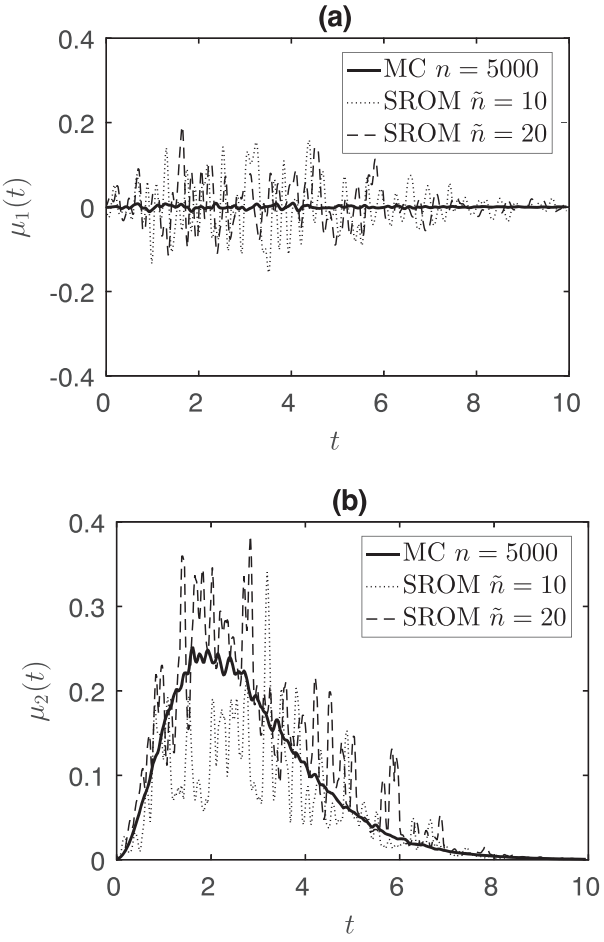

FIGURE 6 Moments $\mu(t, q)$ and its stochastic reduced-order model estimates $\tilde{\mu}(t, q)$ for (a) $q = 1$ and (b) $q = 2$, for $n = 5,000$, $\tilde{n} = 10$, and $\tilde{n} = 20$, for $A(t)$ calculated using $(m, r) = (6.3, 30km)$

$$\tilde{F}(x; t) = \sum_{k=1}^{\tilde{n}} p_k \mathbf{1}\left\{\tilde{a}_k(t) \leq x\right\}, \tag{5}$$

$$\tilde{\mu}(t; q) = \sum_{k=1}^{\tilde{n}} p_k \tilde{a}_k^q(t), \tag{6}$$

$$\tilde{\Sigma}(t, s) = \sum_{k=1}^{\tilde{n}} p_k \tilde{a}_k(t)\tilde{a}_k(s). \tag{7}$$

Figure 5 shows (a) the MC estimators of the marginal distribution of $A(t)$ calculated with $n = 5,000$ samples and the respective approximate SROM estimators $\tilde{F}(x, t)$ of $\tilde{A}(t)$ for (b) $\tilde{n} = 10$ and (c) $\tilde{n} = 20$, for $A(t)$ calculated for $(m, r) = (6.3, 30km)$.

Panels (a) and (b) of Figure 6 show the first two-order moments, that is, $\mu(t, 1)$ and $\mu(t, 2)$, of the process $A(t)$ calculated by the MC estimators with $n = 5,000$ samples and for the SROM $\tilde{A}(t)$, with $\tilde{n} = 10$ and $\tilde{n} = 20$, respectively. Finally, Figure 7 illustrates (a) the MC estimator of the covariance function $\Sigma(t, s)$ of $A(t)$ calculated with $n = 5,000$ samples and the SROM estimators $\tilde{\Sigma}(t, s)$ of $\tilde{A}(t)$ for (b) $\tilde{n} = 10$ and (c) $\tilde{n} = 20$, respectively.

In Figures 5-7, it can be noticed that all SROM statistics are improving as the dimension $\tilde{n}$ increases from 10 to 20, a value for which they approach the MC target statistics within a reasonable accuracy. A further discussion on the topic of the SROM accuracy is presented in the following section. More importantly, a sensitivity analysis on how the MC estimates of $\varphi(\nu_D; \zeta_D)$ in Equation 2 compare with the SROM approximates is also provided. As shown herein, the SROM is built based on the target samples statistics of the input, independent of the system subjected to it, and thus, the system used as an example in Equation 1 can be replaced by any other customary structure.

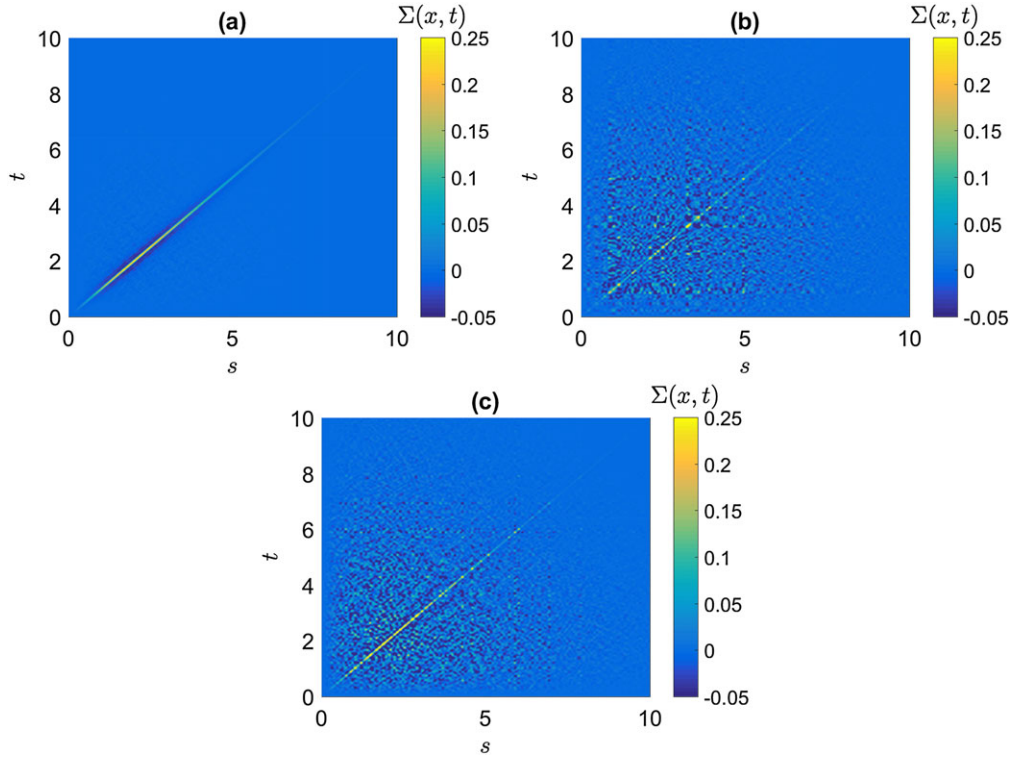

FIGURE 7 Covariance functions (a) $\Sigma(t,s)$ for $n = 5,000$ samples of $A(t)$; and the stochastic reduced-order model estimates $\tilde{\Sigma}(t,s)$ for (b) $\tilde{n} = 10$ and (c) $\tilde{n} = 20$, for $A(t)$ calculated using $(m,r) = (6.3, 30km)$

3.3 | Sensitivity analysis

The performance of $\tilde{A}(t)$ depends on the SROM's size $\tilde{n}$, and for a given $\tilde{n}$, the accuracy of the SROM depends on its construction, that is, the selection of samples $\tilde{a}_k(t)$ and their probabilities p_k. Thus, increasing the dimension of the SROM $\tilde{n} \to \infty$ would produce very accurate statistics of the process $A(t)$, as it converges to the MC solution,[59,78] but it comes at a large computational cost. However, the real gain of using SROMs can only be judged with respect to the response statistics, mainly the metric $\varphi(\nu_D;\zeta_D)$ in Equation 2 used for the design of the TID's parameters $(\nu_D;\zeta_D)$. The accuracy of the response statistics for $X(t)$ depends on that of $\tilde{A}(t)$ and the assumption that samples of $\tilde{a}_k(t)$ map into samples of $\tilde{x}_k(t)$ with same probabilities p_k, by solving Equation 1. Figure 8a shows the tail distribution functions $1 - F_X(x)$ of $X(t)$ calculated for earthquakes with parameters $(m,r) = (6.3, 30km)$ and a range of parameters $\nu_D \in [0, 8\pi]\, rad/s$ and $\zeta_D \in [0, 0.3]$, respectively, while panel (b) shows the respective plot of $\varphi(\nu_D;\zeta_D)$ for $x_{cr} = 0.02$. The bold line in Figure 8a marks the tail distribution function corresponding to parameters (ν_D,ζ_D) selected for the design of the TID for earthquakes characterized by $(m,r) = (6.3, 30km)$, that is, the values (ν_D,ζ_D) for which the minimum of $\varphi(\nu_D;\zeta_D)$ is achieved. Note that the plots in Figure 8 are calculated using MC simulations with $n = 5,000$ samples of $A(t)$ for $(m,r) = (6.3, 30km)$.

Accurate SROM response statistics have been achieved in previous studies[78] with low values of $\tilde{n}$. The SROM estimate $\tilde{\varphi}(\nu_D;\zeta_D)$ of $\varphi(\nu_D;\zeta_D)$ is calculated as in Equation 2 by using samples $x_k(t) = \{x_{k,i}, i = 1, \ldots, N_{dof} + 1\}$ corresponding to the SROM $\{(a_k(t), p_k), \quad k = 1, \ldots, \tilde{n}\}$, as follows:

$$\tilde{\varphi}(\nu_D,\zeta_D) = \int_{x_{cr}}^{\infty} (1 - F_{\tilde{X}}(x))\, dx, \tag{8}$$

where $F_{\tilde{X}}(x) = \sum_{k=1}^{\tilde{n}} p_k \mathbf{1}\{\max_{t\geq 0}|\tilde{x}_{k,1}(t)| \leq x\}$ is the SROM estimator for the response probability distribution function.

Figure 9 shows the contour plot of the MC estimate of $\varphi(\nu_D,\zeta_D)$ from Figure 8b in solid lines, together with the corresponding SROM approximates $\tilde{\varphi}(\nu_D,\zeta_D)$, in dashed lines, calculated with the SROM $\tilde{A}(t)$ with dimension $\tilde{n} = 10$ (panel [a] and $\tilde{n} = 20$ (panel [b]), for the same earthquake with parameters $(m,r) = (6.3, 30km)$. The circle marks the design values (ν_D,ζ_D) calculated by MC, whereas the dark sign marks the same values calculated by the SROM. For comparison with

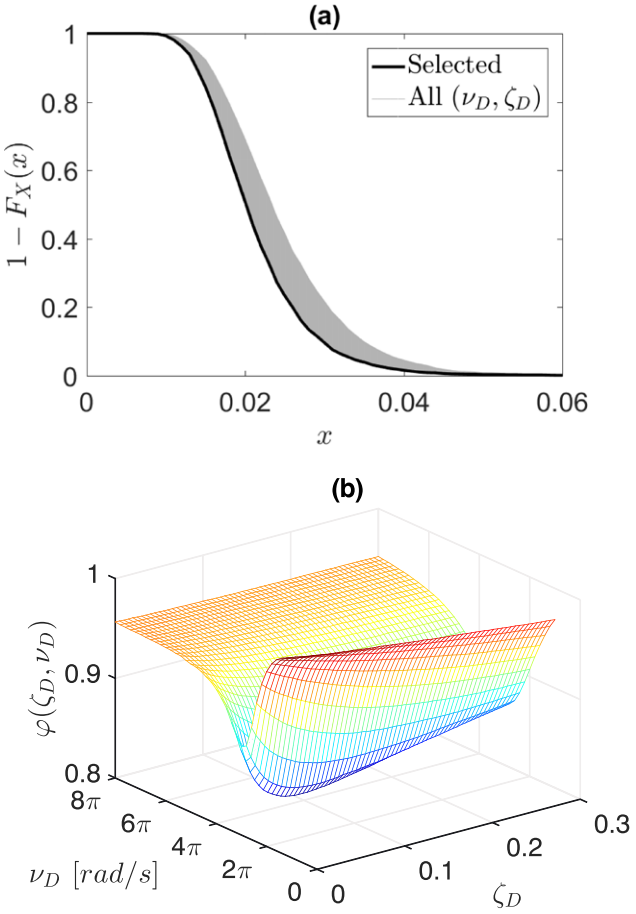

FIGURE 8 (a) The tail distribution function $1 - F_X(x)$ of $X(t)$; (b) the design metric $\varphi(\nu_D; \zeta_D)$ for $x_{cr} = 0.02$, $\nu_D \in [0, 8\pi] rad/s$, $\zeta_D \in [0, 0.3]$, and earthquakes with parameters $(m, r) = (6.3, 30km)$

previous benchmark studies of the TID, two additional values of (ν_D, ζ_D) corresponding to the deterministic harmonic approach developed in the study of Lazar et al.,[8] and to Den Hartog's approach,[5] are illustrated.

It is important to notice in Figure 9 that the SROM estimates of (ν_D, ζ_D) are reliable and that a SROM dimension of $\tilde{n} = 20$ produces results nearly identical with the MC estimate. The errors of SROM statistics are bounded with bounds established by Warner et al.[76] and Uy and Grigoriu,[62] but this analysis is beyond the scope of this paper.

4 | FULL SITE-SEISMICITY DESIGN

The previous section established the effect of TID parameter selection on the structural response to a $(m, r) = (6.3, 30km)$ earthquake. We now extend our study to consider the full range of (m, r) values in the SAM that characterises the chosen site as established in Section 3. The design methodology for TIDs proposed in this study takes into the account that the seismic ground-motions' frequency contents are functions of (m, r) as shown in Figure 4 and that the structural response is highly sensitive to this frequency content. Figure 10 shows the design parameters (ν_D, ζ_D) obtained using the stochastic estimator in Equation 8, compared with the harmonic and Den Hartog deterministic estimates for three different types of earthquakes: (a) $(m, r) = (6.3, 30km)$; (b) $(m, r) = (6.7, 30km)$; (c) $(m, r) = (8.1, 110km)$.

The deterministic approaches are insensitive to the types of earthquakes, whereas the TID design parameters can vary significantly with respect to (m, r). In most of the cases tested, the frequency estimates ν_D do not vary significantly from the deterministic values. However, large discrepancies may be noticed in the damping ratios ζ_D with respect to the deterministic results, which in the most of the cases are conservative. Given that only one value of (ν_D, ζ_D) can be selected for the design of a TID, the (m, r)-dependence of (ν_D, ζ_D) is impractical. Thus, for a comprehensive design of the TID with respect to the seismicity at a site, a SROM $\tilde{A}(t)$ must be constructed, and $\tilde{\varphi}_{m,r}(\nu_D, \zeta_D)$ in Equation 8 must be calculated

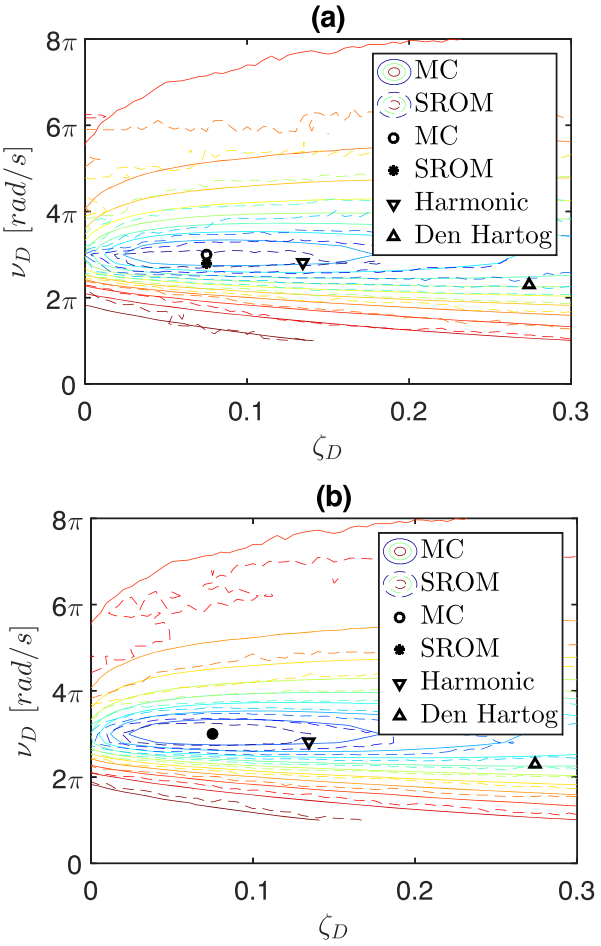

FIGURE 9 MC estimate $\varphi(\nu_D, \zeta_D)$ versus stochastic reduced-order model estimates $\tilde{\varphi}(\nu_D, \zeta_D)$, for (a) $\tilde{n} = 10$ and (b) $\tilde{n} = 20$, using $(m, r) = (6.3, 30km)$

for each (m, r) in the SAM (see Figure 2). The values for the design of the TID will be calculated by minimizing the cost function $\varphi_{SAM}(\nu_D, \zeta_D)$ defined for the entire site seismicity, that is, for the entire SAM:

$$\varphi_{SAM}(\nu_D, \zeta_D) = \sum_{(m,r)} \tilde{\varphi}_{m,r}(\nu_D, \zeta_D)\mathbf{P}\{(M, R) = (m, r)\}, \tag{9}$$

where $\sum_{(m,r)}$ defines the summation over all the values (m, r) in the SAM. Note that $\tilde{\varphi}_{m,r}(\nu_D, \zeta_D)$ needs to be calculated only for (m, r) pairs for which $\mathbf{P}\{(M, R) = (m, r)\} > 0$. Similarly to Figure 10, Figure 11a shows the metric $\varphi_{SAM}(\nu_D, \zeta_D)$ and indicates the minimum value of the design parameters (ν_D, ζ_D), with respect to the same deterministic values.

Figure 11b shows the probability tail distribution functions $1 - F_{\tilde{X}}(x)$ for the values (ν_D, ζ_D) calculated for each (m, r) in the SAM. The bold solid line shows the final tail distribution function for the response of the controlled system with the selected design parameters, corresponding to the minimum value in panel (a) that considers the distinct likelihoods of earthquakes in the SAM in Figure 2. The bold dashed line shows the mean function $1 - F_{\tilde{X}}(x)$ calculated by using the mean TID parameters for each (m, r) in the SAM, for which $\mathbf{P}\{(M, R) = (m, r)\} > 0$, that is, assuming that all earthquakes in the SAM are equally likely to occur. This shows that simply taking the average of (ν_D, ζ_D) over (m, r) can result in significant underestimating the response of the structure.

To assess further these results, the following analysis of the TID-controlled system subjected to the real ground-motion records in the NGA-West data set[73] is now considered. This data set contains approximately 3,500 time histories of different magnitudes, source-to-site distances, and recorded at various sites characterized by different values of v_{s30}. Figure 12 shows scatter plots for each record in the data set that has a maximum absolute displacement of the uncontrolled system greater than or equal to 0.005, for the case where the optimal (ν_D, ζ_D), we selected using the proposed stochastic approach and the harmonic and Den Hartog approaches, as shown in Figure 11.

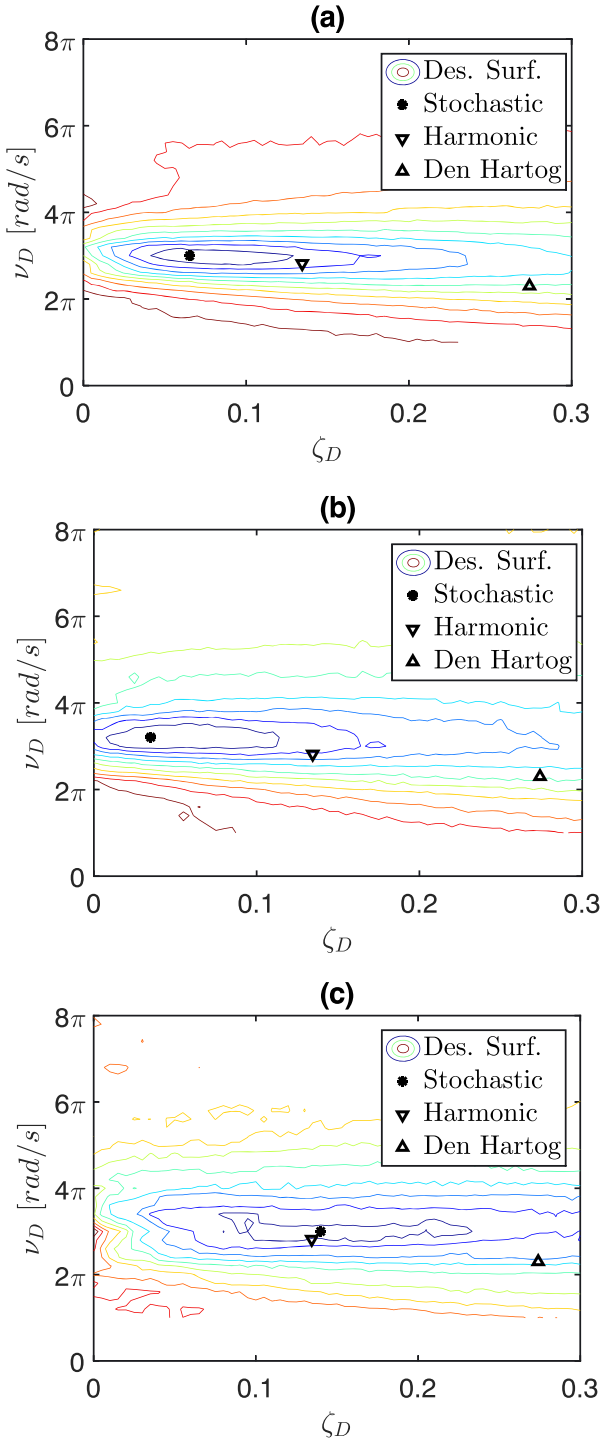

FIGURE 10 Contour plots of the deign surfaces (Des. Surf.) of $\varphi_{SAM}(\nu_D, \zeta_D)$ for (a) $(m, r) = (6.3, 30km)$; (b) $(m, r) = (6.7, 30km)$; (c) $(m, r) = (8.1, 110km)$

Figure 12a compares the maximum absolute displacements of the uncontrolled versus the TID-controlled systems for all three designs with parameters shown in Figure 11a, that is, the SROM stochastic approach, and the deterministic harmonic and Den Hartog approaches are tested for the design of the TID. Note that the points above the dashed lines show records for which the TID-controlled system underperforms with respect to the uncontrolled system, that is, fails to provide a lower maximum absolute displacement.

Figure 12b shows the percentage differences between the maximum absolute displacements of the uncontrolled and TID-controlled systems, normalised by the uncontrolled displacements, for all three TID designs as in panel (a). Note

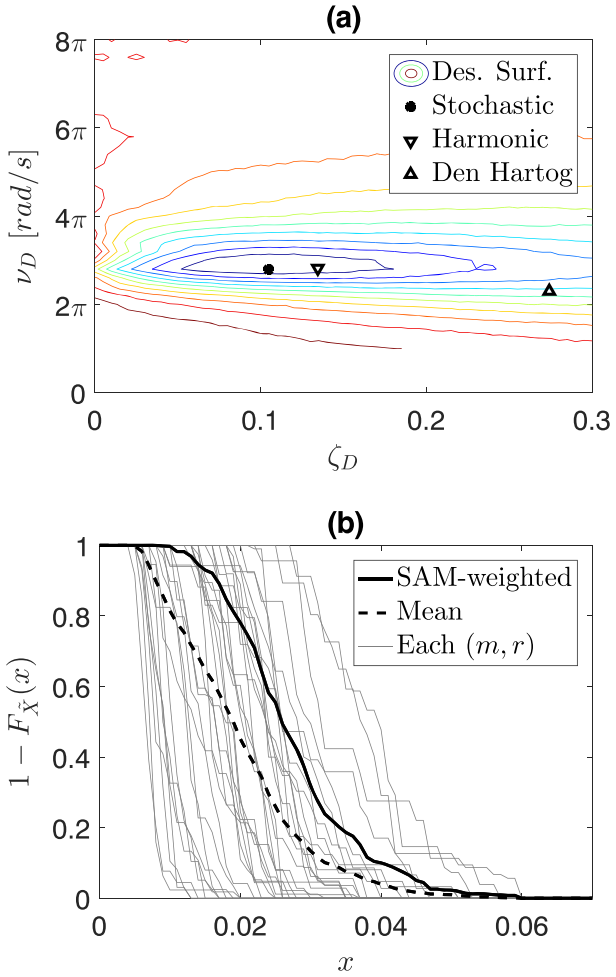

FIGURE 11 (a) Design contour of $\varphi_{SAM}(\nu_D, \zeta_D)$ accounting for all (m, r) across the SAM and (b) corresponding tail distribution functions for (m, r) values

also that a negative value, that is, a point below the dashed line, illustrates a record for which the TID-controlled system underperforms when compared with the uncontrolled system. The solid lines in Figure 12b are regression lines for the percentage differences for each of the three TID designs analysed.

Qualitatively, from Figure 12, it can be inferred that the stochastic and the harmonic designs of the TID perform similarly, for the system and site considered in this study. Furthermore, the reduction in the structural response through these two designs of the TID is larger than in the case of the Den Hartog design, as it is seen in both plots. Quantitative results regarding the stochastic and the two deterministic designs of the TID for the NGA-West analyses shown in Figure 12 are presented in Table 1. This table, as well as Figure 11a, shows that all three designs of the TID have notable differences in the damping ratios ζ_D, for similar frequency values ν_D. More specifically, the differences in the performances of the TID-controlled systems are further expressed as the average percentage of successes, that is, the ratio between the number of records for which the TID-controlled systems exhibit lower maximum absolute displacements than the uncontrolled systems. Another metric used for this comparison is the average damage reduction, which is the mean ratio between the maximum absolute displacements of the TID-controlled system and the uncontrolled system.

Whereas the Den Hartog design of the TID-controlled system fails to provide improved responses only in 3.5% of the cases, the other two designs fail in approximately 9% of the cases but provide better responses by reducing the maximum absolute responses by approximately 15%, rather than only 10% in the case of the Den Hartog design. Finally, the stochastic framework proposed for the design of the TIDs is able to provide rigorous values consistent with the seismic hazard at a site. However, in the current example, of the seismic hazard in Los Angeles and the MDOF structure considered, the stochastic and the deterministic harmonic designs provide TID designs with similar performances. Nevertheless, the performance-based framework proposed does provide a better understanding on how the TID performs with respect to different earthquakes, inputs with complex various frequency contents, and it can make a significant difference as, for

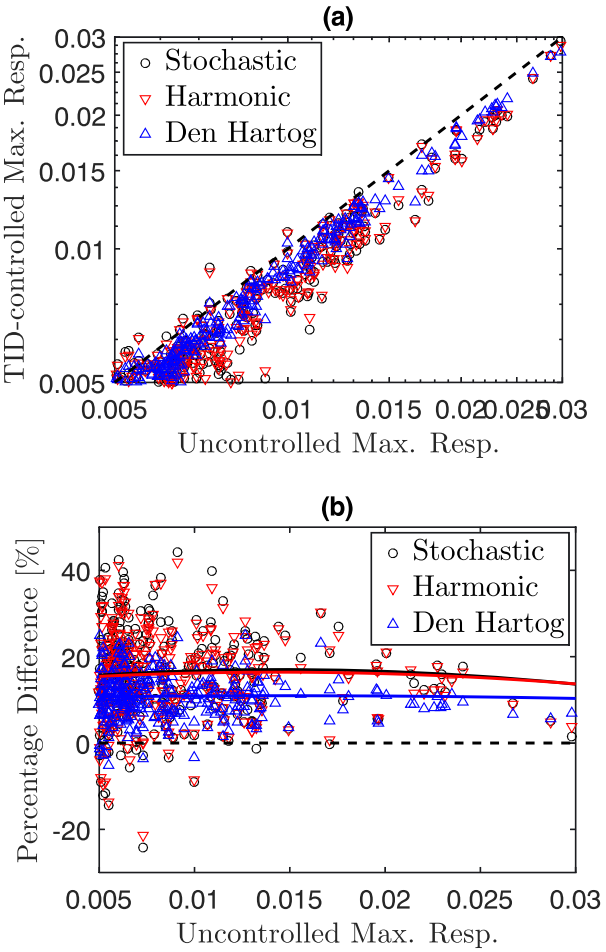

FIGURE 12 (a) Maximum absolute responses of the TID-controlled versus uncontrolled structures subjected to the records in the NGA-West database, and (b) corresponding percentage differences, for the stochastic and the deterministic benchmark designs

TABLE 1 Methods comparison

Comparison item	Stochastic	Harmonic	Den Hartog
ζ_D	0.105	0.134	0.274
$\nu_D[rad/s]$	8.797	8.819	7.201
ADR	14.7%	14.6%	10.5%
APS	90.2%	91.5%	96.5%

Note. ADR: average damage reduction; APS: average percentage of successes.

example, in the case shown in Figure 9b, where the damping ratio ν_D of the TID is only 2%, rather than 13% as in the case of the harmonic design. Moreover, this study provides a highly efficient framework for the stochastic design of the TID that provides reliable robust results with a computational effort smaller by a factor of 250 than the same result obtained by MC, or in absolute values, for a SAM of 200 (m, r) pairs as in the example herein, the number of dynamic analyses is reduced from one million to only 4,000.

5 | CONCLUSIONS

A novel methodology based on SROMs is proposed for the fully probabilistic design of TIDs with respect to their performance in civil engineering structures subjected to seismic loads. The framework is general, and the TID is designed for nonlinear MDOF structures, subjected to synthetic nonstationary, non-Gaussian seismic ground motions. The design

parameters of the TID using the methodology proposed are consistent with the classical methodology for probabilistic design, based on MC simulations. The design framework proposed is computationally efficient, robust, and easy to use. This method allows a fully probabilistic design of the TID to account for the site seismicity, by accounting for the character of ground motions with respect to seismic-source and local site characteristics. Finally, results obtained are compared with deterministic benchmark approaches, which shows that the probabilistic design may lead to more economical results for certain types of earthquakes, while preserving the performance of the more conservative deterministic approaches currently used in control engineering.

ACKNOWLEDGEMENTS

The work presented in this paper by A. Radu has been supported by the Marie Skłodowska-Curie Actions of the European Union's Horizon 2020 Program under the grant agreement 704679 - PARTNER. S. A. Neild would like to acknowledge the support of the EPSRC through fellowship EP/K005375/1. The support from these fellowships is gratefully acknowledged.

ORCID

Alin Radu https://orcid.org/0000-0003-0301-3539
Irina F. Lazar https://orcid.org/0000-0002-4456-0910

REFERENCES

1. Aguirre JJ, Almazan JL, Paul CJ. Optimal control of linear and nonlinear asymmetric structures by means of passive energy dampers. *Earthq Eng Struct Dyn*. 2013;42(3):377-395.
2. Soong TT, Spencer BF Jr. Supplemental energy dissipation: state-of-the-art and state-of-the-practice. *J Eng Struct*. 2002;24:243-259.
3. Soong TT, Cimellaro GP. Future directions in structural control. *Struct Control Health Monit*. 2009;16:7-16.
4. Frahm H. Device for damping vibrations of bodies. Specification of Letters Patent, no US989958 A; 1909.
5. DenHartog J. *Mechanical Vibrations*. New York: McGraw-Hill; 1947.
6. Miranda JC. On tuned mass dampers for reducing the seismic response of structures. *Earthq Eng Struct Dyn*. 2005;34:847-865.
7. Marian L, Giaralis A. Optimal design of a novel tuned mass-damper–inerter (TMDI) passive vibration control configuration for stochastically support-excited structural systems. *Probab Eng Mech*. 2014;38:156-164.
8. Lazar IF, Neild S, Wagg D. Using an inerter-based device for structural vibration suppression. *Earthq Eng Struct Dyn*. 2014;43(8):1129-1147.
9. Smith MC. Synthesis of mechanical networks the inerter. *IEEE Trans Autom Control*. 2002;47:1648-1662.
10. Ikago K, Saito K, Inoue N. Seismic control of single-degree-of-freedom structure using tuned viscous mass damper. *Earthq Eng Struct Dyn*. 2012;41(3):453-474.
11. Sugimura Y, Goto W, Tanizawa H, et al. Response control effect of steel building structure using tuned viscous mass damper. In: Proceedings of the 15th World Conference on Earthquake Engineering; 2012; Lisbon, Portugal:24-28.
12. Zhang SY, Jiang JZ, Neild S. Optimal configurations for a linear vibration suppression device in a multi-storey building. *Struct Control Health Monit*. 2017;24(3):e1887.
13. Lazar I, Neild S, Wagg D. Vibration suppression of cables using tuned inerter dampers. *Eng Struct*. 2016;122:62-71.
14. Gonzalez-Buelga A, Lazar IF, Jiang JZ, Neild SA, Inman DJ, Assessing the effect of nonlinearities on the performance of a tuned inerter damper. *Structural Control and Health Monitoring*. 2017;24(3):e1879. e1879 STC-15-0213.R1.
15. De Domenico D, Ricciardi G. Improving the dynamic performance of base-isolated structures via tuned madd damper and inerter devices: A comparative study. *Struct Control Health Monit*. 2018;25:e2234. https://doi.org/10.1002/stc.2234
16. Deastra P, Wagg DJ, Sims ND. The effect of a tuned-inerter-damper on the seismic response of base-isolated structures. In: 16th European Conference on Earthquake Engineering; 2018; Thessaloniki, Greece:18-21.
17. Zhang XJ, Ahmadian M, Guo KH. On the benefits of semi-active suspensions with inerters. *J Shock Vib*. 2012;19:257-272.
18. Hu Y, Chen MZQ. Low-complexity passive vehicle suspension design based on element-number-restricted networks and low-order admittance networks. *J Dyn Syst Meas Control*. 2018;140(10):101014-1–101014–7.
19. Li P, Lam J, Cheung KC. Control of vehicle suspension using an adaptive inerter. *Proc Inst Mech Eng D J Automob Eng*. 2015;229(4):1934-1943.
20. Wang FC, Liao MK. The lateral stability of train suspension systems employing inerters. *Int J Veh Mech Mobil*. 2010;48:619-643.
21. Jiang JZ, Matamoros-Sanchez AZ, Goodall RM, Smith MC. Passive suspensions incorporating inerters for railway vehicles. *Veh Syst Dyn*. 2012;50:263-276.
22. Li Y, Jiang JZ, Neild SA. Inerter-based configurations for main-landing-gear shimmy suppression. *J Aircr*. 2017;52(2):684-693.
23. Radu A, Grigoriu M. A site-specific seismological model for probabilistic seismic-hazard analysis. *Bull Seismol Soc Amer*. 2014;104(6):3054-3071.
24. Bommer JJ, Acevedo AB. The use of real earthquake accelerograms as input to dynamic analysis. *J Earthq Eng*. 2004;8(1):43-91.

25. Ozer B, Akkar S. A procedure on ground motion selection and scaling for nonlinear response of simple structural systems. *Earthq Eng Struct Dyn*. 2012;41:1693-1707.
26. Baker J. Efficient analytical fragility function fitting using dynamic structural analysis. *Earthq Spectra*. 2015;31(1):579-599.
27. Vamvatsikos D, Cornell C. Incremental dynamic analysis. *Earthq Eng Struct Dyn*. 2002;31:491-514.
28. Kafali C, Grigoriu M. Seismic fragility analysis: application to simple linear and nonlinear systems. *Earthq Eng Struct Dyn*. 2007;36(13):1885-1900.
29. Radu A, Grigoriu M. An earthquake-source-based metric for seismic fragility analysis; 2018.
30. Grigoriu M. To scale or not to scale seismic ground accceleration records. *J Eng Mech*. 2011;137(4):284-293.
31. Rezaeian S, Kiureghian AD. Simulation of orthogonal horizontal ground motion components for specified earthquake and site characteristics. *Earthq Eng Struct Dyn*. 2012;41(2):335-353.
32. Soong T, Grigoriu M. *Random Vibration of Mechanical and Structural Systems*. New Jersey, USA: PTR Prentice - Hall, Inc; 1993.
33. Hu Y, Chen MZQ, Shu Z, Huang L. Analysis and optimisation for inerter-based isolators via fixed-point theory and algebraic solution. *J Sound Vib*. 2015;346:17-36.
34. Krenk S, Hogsberg J. Tuned resonant mass or inerter-based absorbers: unified calibration with quasi-dynamic flexibility and inertia correction. *Proc Royal Soc A*. 2016;472:1-23.
35. Barredo E, Blanco A, Colin J, et al. Closed-form solutions for the optimal design of inerter-based dynamic vibration absorbers. *Int J Mech Sci*. 2018;144:41-53.
36. Taflanidis AA, Scruggs JT, Beck JL. Reliability-based performance objectives and probabilistic robustness in structural control applications. *J Eng Mech*. 2008;134(4):291-301.
37. Giaralis A, Taflanidis AA. Optimal tuned mass-damper-inerter (tmdi) design for seismically excited mdof structures with model uncertainties based on reliability criteria. *Struct Control Health Monit*. 2018;25(2):e2082. e2082 STC-17-0065.R1.
38. Chao P, Ruifu Z. Design of structure with inerter system based on stochastic response mitigation ratio. *Struct Control Health Monit*. 2018;25(6):e2169. e2169 STC-17-0318.R2.
39. Masri SF, Caffrey JP. Transient response of a SDOF system with an inerter to nonstationary stochastic excitation. *ASME J Appl Mech*. 2017;84(4):041005-041005–10. https://doi.org/10.1115/1.4035930
40. Masri SF, Caffrey JP, Hui L. Transient response of MDOF systems with inerters to nonstationary stochastic excitation. *J Appl Mech*; 84(10):101003-101003-13. https://doi.org/10.1115/1.4037551,2017
41. Wang F-C, Su W-J. Impact of inerter nonlinearities on vehicle suspension control. *Veh Syst Dyn*. 2008;46(7):575-595.
42. Bazzurro P, Cornell CA, Shome N, Carballo JE. Three proposals for characterizing mdof nonlinear seismic response. *J Struct Eng*. 1998;124(11):1281-1289.
43. Peter F. Capacity spectrum method based on inelastic demand spectra. *Earthq Eng Struct Dyn*. 1999;28(9):979-993.
44. Jorge R-G, Eduardo M. Inelastic displacement ratios for evaluation of existing structures. *Earthq Eng Struct Dyn*. 2003;32(8):1237-1258.
45. Der KA, Kazuya F. Nonlinear stochastic dynamic analysis for performance-based earthquake engineering. *Earthq Eng Struct Dyn*. 2009;38(5):719-738.
46. Kougioumtzoglou IA, Spanos PD. An approximate approach for nonlinear system response determination under evolutionary stochastic excitation. *Curr Sci*. 2009;97(8):1203-1211.
47. Spanos PD, Evangelatos GI. Response of a non-linear system with restoring forces governed by fractional derivatives—time domain simulation and statistical linearization solution. *Soil Dyn Earthq Eng*. 2010;30(9):811-821. Special Issue in honour of Prof. Anestis Veletsos.
48. Sanjay L, Marsden JE, Sonja G. A subspace approach to balanced truncation for model reduction of nonlinear control systems. *Int J Robust Nonlinear Control*. 2002;12(6):519-535.
49. Kerschen G, Golinval J-c, Vakakis AF, Bergman LA. The method of proper orthogonal decomposition for dynamical characterization and order reduction of mechanical systems: An overview. *Nonlinear Dyn*. 2005;41:147-169.
50. Shadab Far M, Wang Y. Approximation of the Monte Carlo sampling method for reliability analysis of structures. *Math Probl Eng*. 2016;2016(05):1-9.
51. Yin Y, Neild SA, Jiang JZ, Knowels JAC, Nie H. Optimization of a main landing gear locking mechanism using bifurcation analysis. *J Aircr*. 2017;54(6):2126-2139.
52. Yang X, Choi M, Lin G, Karniadakis GE. Adaptive anova decomposition of stochastic incompressible and compressible flows. *J Comput Phys*. 2012;231:1587-1614.
53. Li X, Du D, Pei J, Menhas M. Probabilistic load flow calculation with latin hypercube sampling applied to grid-connected induction wind power system. *Trans Inst Meas Control*. 2013;35(1):56-65.
54. Grigoriu M. *Stochastic Calculus: Applications in Science and Engineering*. USA: Birkhäuser; 2002.
55. Zhang R, Elishakoff I, Shinozuka M. Analysis of nonlinear sliding structures by modified stochastic linearization methods. *Nonlinear Dyn*. 1994;5:299-312.
56. Hijawi M, Ibrahim RA, Moshchuk N. Nonlinear random response of ocean structures using first- and second-order stochastic averaging. *Nonlinear Dyn*. 1997;12:155-197.
57. Kuether RJ, Deaner BJ, Hollkamp JJ, Allen MS. Evaluation of geometrically nonlinear reduced-order models with nonlinear normal modes. *AIAA J*. 2015;53(11):3273-3285.
58. Haller G, Ponsioen S. Nonlinear normal modes and spectral submanifolds: existence, uniqueness and use in model reduction. *Nonlinear Dyn*. 2016;86:1-42.

59. Grigoriu M. Reduced order models for random functions. Application to stochastic problems. *Appl Math Model*. 2009;33:161-175.
60. Grigoriu M. Linear random vibration by stochastic reduced-order models. *Int J Numer Methods Eng*. 2010;82(12):1537-1559.
61. Grigoriu M. A method for solving stochastic equations by reduced order models and local approximations. *J Comput Phys*. 2012;231:6496-6513.
62. Uy WIT, Grigoriu MD. An adaptive method for solving stochastic equations based on interpolants over voronoi cells. *Probab Eng Mech*. 2018;51:23-41.
63. Waltering M, Bungard V, Waldmann D, Zurbes A, Maas S, De Roeck G. Damage assessment of civil engineering structures by the observation of non-linear dynamic behaviour. In: International Conference on Experimental Vibration Analysis for Civil Engineering Structures - EVACES, Porto, Portugal, 2007:24-26.
64. Radu A, Grigoriu M. A site-specific ground-motion simulation model: application for vrancea earthquakes. *Soil Dyn Earthq Eng*. 2018;111:77-86.
65. USGS. U.S. geological survey: Uniform hazard tool. last checked on 05/11/2018.URL https://earthquake.usgs.gov/hazards/interactive/; 2018.
66. McGuire RK. Probabilistic seismic hazard analysis and design earthquakes: Closing the loop. *Bull Seismol Soc Amer*. 1995;85(5):1275-1284.
67. Bazzurro P, Cornell C. Disaggregation of seismic hazard. *Bull Seismol Soc Amer*. 1999;89(2):501-520.
68. Papageorgiou A, Aki K. A specific barrier model for the quantitative description of inhomoeneous faulting and the prediction of strong ground motion. Applications of the model. *Bull Seismol Soc Amer*. 1983;73(4):953-978.
69. Papageorgiou A, Aki K. A specific barrier model for the quantitative description of inhomoeneous faulting and the prediction of strong ground motion. description of the model. *Bull Seismol Soc Amer*. 1983;73(3):693-722.
70. Deodatis G. Non-stationary stochastic vector processes: Seismic ground motion applications. *Probab Eng Mech*. 1996;11(3):149-167.
71. Halldorsson B, Papageorgiou A. Calibration of the specific barier model to earthquake to different tectonic regions. *Bull Seismol Soc Amer*. 2005;95(4):1276-1300.
72. Tsioulou A, Taflanidis A, Galasso C. Modification of stochastic ground motion models for matching target intensity measures. *Earthq Eng Struct Dyn*. 2017:1-22.
73. Abrahamson N, Atkinson G, Boore D, et al. Comparisons of the nga ground-motion rzelations. *Earthq Spectra*. 2008;24(1):45-66.
74. Vlachos C, Papakonstantinou KG, Deodatis G. Predictive model for site specific simulation of ground motions based on earthquake scenarios. *Earthq Eng Struct Dyn*. 2017;47(1):195-218.
75. Goda K, Petrone C, De Risi R, Rossetto T. Stochastic coupled simulation of strong motion and tsunami for the 2011 Tohoku, Japan earthquake. *Stochastic Environ Res Risk Assess*. 2017;31(9):2337-2355.
76. Warner JE, Grigoriu M, Aquino W. Stochastic reduced order models for random vectors: Application to random eigenvalue problems. *Probab Eng Mech*. 2013;31:1-11.
77. Allen I, Miller C, Rice TR. Discrete approximations of probability distributions. *Manag Sci*. 1983;29(3):352-362.
78. Warner JE, Aquino W, Grigoriu MD. Stochastic reduced order models for inverse problems under uncertainty. *Comput Meth Appl Mech Eng*. 2015;285:488-514.

How to cite this article: Radu A, Lazar IF, Neild SA. Performance-based seismic design of tuned inerter dampers. *Struct Control Health Monit*. 2019;e2346. https://doi.org/10.1002/stc.2346

APPENDIX A

This appendix provides information about the uncontrolled and TID-controlled structures in Sections 2.1 and 2.2, respectively. The structure with a TID mounted at the ground floor, as assumed in this study, is illustrated schematically in Figure A1.

The structure considered in this study has $N_{dof} = 5$ degrees of freedom. The original uncontrolled structure is described by the mass $M = \{m_{i,j}|m_{i,i} = 1; m_{i,j} = 0, i \neq j; i,j = 1, \dots, 5\}$, damping $C = \{c_{i,j}|c_{i,i} = 6.34, i \leq 4; c_{5,5} = 3.05; c_{1,2} = c_{2,1} = -2.84; c_{2,3} = c_{3,2} = -2.84; c_{3,4} = c_{4,3} = -2.84, c_{4,5} = c_{5,4} = -2.84; c_{i,j} = 0, \text{otherwise}; i,j = 1, \dots, 5\}$, and stiffness $K = \{k_{i,j}|k_{i,i} = 2000, i \leq 4; k_{5,5} = 1000; k_{1,2} = k_{2,1} = -1000; k_{2,3} = k_{3,2} = -1000; k_{3,4} = k_{4,3} = -1000, k_{4,5} = k_{5,4} = -1000; k_{i,j} = 0, \text{otherwise}; i,j = 1, \dots, 5\}$ matrices in Equation 1. The nonlinear coefficient is $\rho = -0.3$.

For the TID-controlled system, the mass M, damping C, and stiffness K matrices in the equation of motion Equation 1 are replaced by $M^{(d)}$, $C^{(d)}$, and $K^{(d)}$ of the structural system equipped with the TID. Note that the new matrices for the TID-controlled structure have $N_{dof} + 1 = 6$ degrees of freedom, the additional one being introduced by the TID, and are described in detail in Section 2.2. For a better understanding of how the TID affects the behaviour of the host structure, the matrix forms of $M^{(d)}$, $C^{(d)}$ and $K^{(d)}$ are provided below as functions of the original mass, damping and stiffness matrices M, C and K:

$$M^{(d)} = \begin{pmatrix} & & 0 \\ & (M) & 0 \\ & & \vdots \\ & & 0 \\ 0 & 0 \ \dots \ 0 & m_d \end{pmatrix},$$

$$C^{(d)} = \begin{pmatrix} c_d & 0 & \dots & 0 & -c_d \\ 0 & & & & 0 \\ \vdots & & \left(O_{N_{dof}-2}\right) & & \vdots \\ 0 & & & & 0 \\ -c_d & 0 & \dots & 0 & c_d \end{pmatrix} + \begin{pmatrix} & & 0 \\ & (C) & 0 \\ & & \vdots \\ & & 0 \\ 0 & 0 \ \dots \ 0 & 0 \end{pmatrix}.$$

The updated stiffness matrix has the same layout as $C^{(d)}$, where c_d is replaced by k_d and C is replaced by K.

$$K^{(d)} = \begin{pmatrix} k_d & 0 & \dots & 0 & -k_d \\ 0 & & & & 0 \\ \vdots & & \left(O_{N_{dof}-2}\right) & & \vdots \\ 0 & & & & 0 \\ -k_d & 0 & \dots & 0 & k_d \end{pmatrix} + \begin{pmatrix} & & 0 \\ & (K) & 0 \\ & & \vdots \\ & & 0 \\ 0 & 0 \ \dots \ 0 & 0 \end{pmatrix},$$

where $O_{N_{dof}-2}$ denotes a zero square matrix of dimension $N_{dof} - 2$. The construction of matrices $M^{(d)}$, $C^{(d)}$ and $K^{(d)}$ require the use of the TID parameters $\theta_D = [m_D, \nu_D, \zeta_D]$, where $m_D = \mu_D \sum_{i=1}^{N_{dof}} m_{i,i} = 5\mu_D$, $c_D = 2\zeta_D \nu_D m_D$, and $k_D = \nu_D^2 m_D$. Coefficient $\mu_D = 20\%$, as assumed and described in Section 2.2, while $\nu_D \in [0, 8\pi] rad/s$ and $\zeta_D \in [0, 0.3]$. The TID design parameters for the problem discussed herein can be collected from Figure 11 (a).

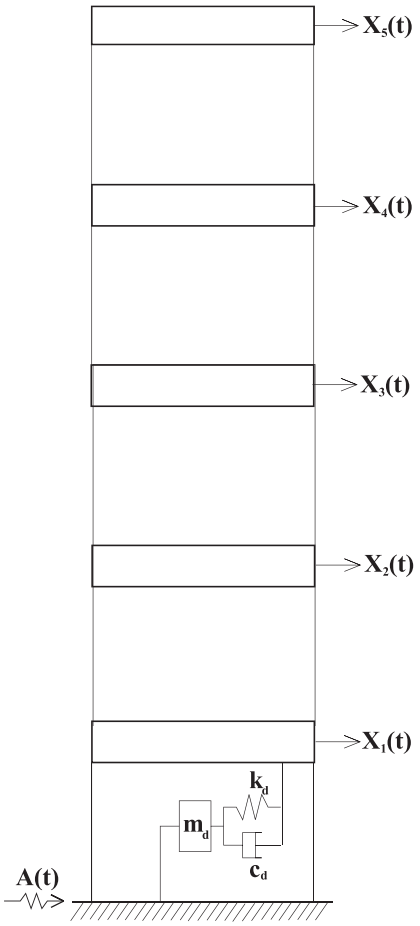

FIGURE A1 TID-controlled structure